Optimizing the Post Sandvik Nanoflex material model using inverse optimization and the finite element method.

T. van Amstel[2],M. Groen[2] ,J. Post[2], J. Huétink[1]

[1]*Faculty of Engineering Technology, University of Twente, P.O. Box 217, 7500 AE Enschede, Netherlands*
URL: www.tm.ctw.utwente.nl *e-mail: j.huetink@ctw.utwente.nl*

[2]*Philips Advanced Technology Centre, P.O. Box 20100, 9200 CA Drachten, Netherlands*
URL: www.philips.com *e-mail: j.post@philips.com*

ABSTRACT: This article describes an inverse optimization method for the Sandvik Nanoflex steel in cold forming processes. The optimization revolves around measured samples and calculations using the Finite Element Method. Sandvik Nanoflex is part of the group of meta-stable stainless steels. These materials are characterized by a good corrosion resistance, high strength, good formability and crack resistance. In addition, Sandvik Nanoflex has a strain-induced transformation and, depending on austenising conditions and chemical composition, a stress-assisted transformation can occur. The martensite phase of this material shows a substantial aging response. The inverse optimization is a sub-category of the optimization techniques. The inverse optimization method uses a top down approach, as the name implies. The starting point is a prototype state where the current state is to converge on. In our experiment the test specimen is used as prototype and a calculation result as current state. The calculation is then adapted so that the result converges towards the test example. An iterative numerical optimization algorithm controls the adaptation. For the inverse optimization method two parameters are defined: shape of the product and martensite profile. These parameters are extracted from both calculation and test specimen, using Fourier analysis and integrals. An optimization parameter is then formulated from the extracted parameters. The method uses this optimization parameter to increase the accuracy of ”The Post” material model for Sandvik Nanoflex. [1] The article will describe a method to optimize material models, using a combination practical experiments, Finite Element Method and parameter extraction.

Key words: finite elements, inverse method, Nanoflex, parameter extraction

1 INTRODUCTION

As companies use more complex material to satisfy increasing costumer demand for high end products and shorter time to markets. Industry demands more powerful development tools to engineer cold forming products. One of the most important developments within this increasing demand for development tools is the finite element method in conjunction with complex material models. In order to create reliable and accurate complex material models it is essential to develop methods that optimize these material models.
In this article an inverse method is presented that optimizes the Post Sandvik Nanoflex model. The inverse method is a top down approach. It is build around converging the current state, from an initial guess, towards the prototype state. This is done with parameter extraction and a numerical iterative optimization routine. For the current state finite element calculations with the Post model are done. The prototype state is given by a measured sample of a product cross section. The calculations are done with the Crystal non linear finite element solver and the program outlay is written in the Matlab programming language.

2 THE MATERIAL MODEL FOR SANDVIK NANOFLEX

Sandvik Nanoflex belongs to the category of metastable austenitic stainless steels. It is also a precipitation hardenable steel, which means that the martensite phase can be aged [2, 3]. For the chemical

	C+N	Cr	Ni	Mo	Ti	Al	Si	Cu
Nanoflex	$\leq$0.05	12.0	9.0	4.0	0.9	0.40	$\leq$0.5	2.0

Table 1: Chemical composition of Sandvik Nanoflex™steel[2]

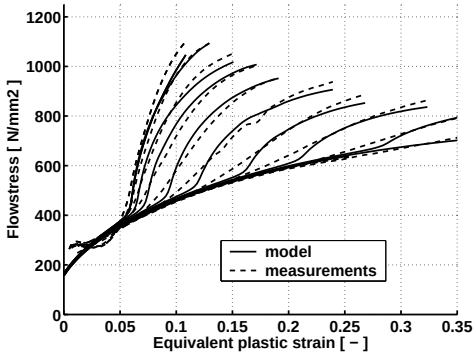

Figure 1: The fitted flow stress model and measured data.

composition, see Table 1.
Depending on the stability of the steel, two phenomena occur:

- a stress-assisted transformation, below the flow stress of the composite,
- a strain-induced transformation, above the flow-stress of the composite at higher temperatures above the martensite start temperature M_s^{σ}.

These transformations are stress state and temperature dependent.

2.1 Strain-induced transformation

The following equation is used to describe the strain-induced transformation:

$$\dot{\varphi}_{\text{strain}} = C_{\text{strain}}(T,\sigma^{\text{H}},Z)[(D_1+\varphi)^{n_1}(f-\varphi)^{n_2}]\dot{\varepsilon}^{\text{p}}, \quad (1)$$

where φ is the martensite content and C_{strain} is a function that describes the dependence of the transformation on the temperature T, hydrostatic stress σ^{H} and material structure Z. The parameter Z is depends on the annealing conditions before metal forming, the chemical composition and crystal orientation and is treated as a constant for this study, C_{strain} is related to the thermodynamics of the transformation.
In Figures 1 and 2, the simulated and measured flow-stress and martensite content are depicted as function of the equivalent plastic strain rate $\dot{\varepsilon}^{\text{p}}$. The values n_1 and n_2 are fit constants, D_1 is related to the nucleation of the transformation and f is the saturation value of the transformation. In both figures, the most left lines correspond to a temperature of 223 K whereas the most right lines correspond to 423 K.

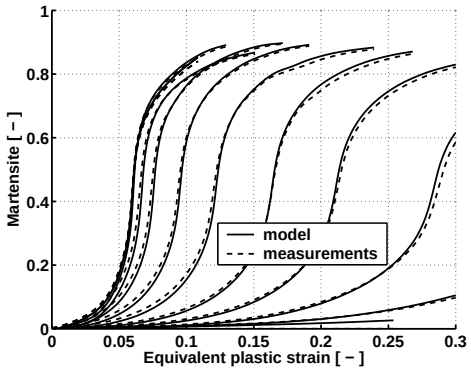

Figure 2: The fitted strain-induced martensite model and measured data.

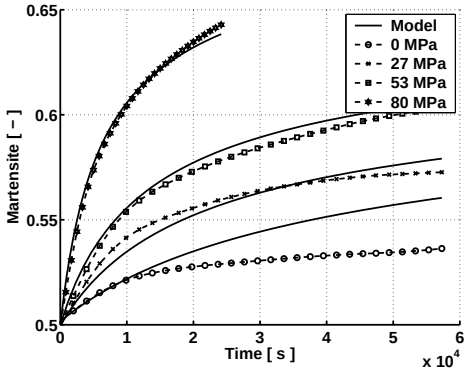

Figure 3: Stress assisted transformation as function of imposed stress level, after plastic pre-straining up to a martensite content of 50%

2.2 Stress-assisted transformation

The description of the stress-assisted transformation is based on [4], but rewritten in a more general form:

$$\begin{aligned}\dot{\varphi}_{\text{stress}} =& C_{\text{stress}}(T,\sigma^{\text{H}},\varepsilon^{\text{p}},Z)[(D_2(Z)+\varphi)^{n_3} \\ & (f_{\text{stress}}(T,\sigma^{\text{H}},\varepsilon^{\text{p}},Z)-\varphi)^{n_4}],\end{aligned} \quad (2)$$

where C_{stress} is a function that describes the dependence of transformation on hydrostatic stress, temperature and material structure. Figure 3 shows the stress assisted transformation after plastic pre-straining (resulting in 50% martensite), as function of the imposed stress level. For the total martensite content we finally get:

$$\dot{\varphi} = \dot{\varphi}_{\text{stress}} + \dot{\varphi}_{\text{strain}} \quad (3)$$

2.3 Post Material model Sandvik Nanoflex

For this study it is assumed that the work hardening depends on plastic strain, martensite content, temperature, and the influence of strain rate. The flow stress of austenite ($i=1$) and martensite ($i=2$) is written

as:

$$\sigma_i^{\mathrm{Y}} = \sigma_{0_i}\sqrt{Y_i}\left(1+\frac{\dot{\varepsilon}^{\mathrm{p}}}{\psi_i}\right)^{\frac{1}{m_i}}. \tag{4}$$

Here, σ_0 is the basic stress which depends on strain rate and temperature, Y is the general dislocation density for one phase, $\dot{\varepsilon}_p$ is the equivalent plastic strain rate, ψ the reference strain rate and m a constant depending on strain rate and temperature. For the combination of both phases the equation becomes

$$\sigma^{\mathrm{Y}} = \sigma_1^{\mathrm{Y}} + \frac{1+\tanh\left(\frac{\varphi-\varphi_0}{q}\right)}{2}(\sigma_2^{\mathrm{Y}} - \sigma_1^{\mathrm{Y}}), \tag{5}$$

where φ_0 and q are introduced to describe the non-linear relation between the flow stresses as a mixture rule. The evolution of the dislocation density in the austenite and martensite is described as follows:

$$\dot{Y}_i = \begin{cases} \left[C_{1i}(C_{2i}-Y_i)^{C_{3i}} + C_{4i}(\dot{\varepsilon}^{\mathrm{p}},T)\right]\dot{\varepsilon}^{\mathrm{p}} & \text{if } Y_i \le C_{2i}, \\ \left[C_{4i}(\dot{\varepsilon}^{\mathrm{p}},T)\right]\dot{\varepsilon}^{\mathrm{p}} & \text{if } Y_i > C_{2i}, \end{cases} \tag{6}$$

where C_{1i}, C_{2i}, C_{3i} are material constants and C_{4i} depends on temperature and strain rate. The constants are not directly related to physical phenomena but are chosen to fit the experiments.
To describe the recovery effect for the dislocation transfer during transformation the following equation is introduced:

$$\dot{Y}_2^{\mathrm{trans}} = \frac{\dot{\varphi}_{\mathrm{strain}}}{\varphi_{\mathrm{strain}}}(C_9(T)Y_1 + C_{10}) - \frac{\dot{\varphi}}{\varphi}Y_2), \tag{7}$$

where C_9 is a constant that depends on temperature and C_{10} depends on the transformation boundary. For more details on the model, the reader is referred to [**?**].

3 EXPERIMENT SETUP

This section describes the Matlab programmed implemented technical layout of the inverse method experiment. The layout consists of a main optimization loop as given in figure 4. This loop incorporates two distinct functionalities that are programmed in series.
The first functionality is a precursor to the second functionality. This first functionality adapts the contour of the computer model to the measured contour. The importance of this is that it gives a common reference for the second functionality. In other words this

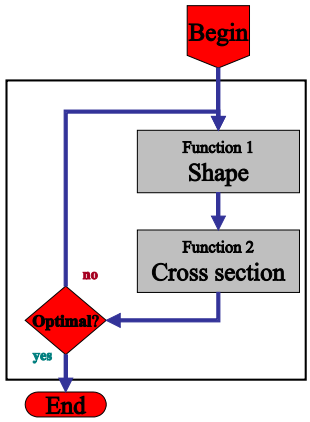

Figure 4: The test Setup. The main loop and the two functionalities are shown.

first functionality ensures that both the model and the measured product have similar product dimensions, so that there can be a good comparison of values over the cross section. The second functionality consists of an adaptation between calculated values and measured values over the cross section of the product. The values that we have optimized range from surface area to a necking profile. These optimizations are placed in different processes, or plug-ins, in serial within the second functionality. It is, off course, possible to expand this range beyond the values we have incorporated to satisfy different requirements. The main loop ends when the results of the functionalities have converged to values that are convenient. This may take a few runs, cause there may be a causal relationship between shape and cross section values. The exact mathematical description of the different parameters is given in sections below. In theory it would be possible to put the two functionalities in parallel and optimize all the parameters at once. Thus converge the entire model towards the measured specimen in one adaptation sequence. But due to significant delays in error correction caused by large required calculation time and better manageability of the serial solution. The experiment uses this serial solution, for now.

4 COMPARISON

4.1 Introduction: Functionality 1

This section presents a method that allows easy comparison of 2-dimensional contours. Shape comparison is needed for the first functionality as described in the test setup section. The method is based on defining a set of invariants that do not variate due to rotation and translation of the contour. These invariants are calculated by: decomposing the contour into a normalized X and Y vectors,

transforming the vectors with a discrete Fourier series to eliminate translation, rejoining the two transformed vectors to eliminate the influence of rotation and finally the interpretation of the created invariants. These invariants allow for comparison between other sets of invariants of different contours. Thus, allowing for accurate and quick comparison between contours.

Note: There are some variants on this method. In the variant we have used for this article the starting point of the vectors X and Y is not arbitrary and must be corresponding with the compared contour.

4.2 Shape comparison

As described in the introduction, the method consists of 4 calculation steps. The first step is of decomposing the original data into two normalized vectors X and Y. First the distance between the points is calculated:

$$D_i = \sqrt{(x_{i+1} - x_i)^2 + (y_{i+1} - y_i)^2} \tag{8}$$

This value is then inserted into the equation 9 to determine the arc length.

$$N_i = \frac{2\Pi\Sigma_{i=1}^{i} D_i}{\Sigma_{i=1}^{N} D_i} \tag{9}$$

The arc length is coupled to the X and Y vectors to create two data sets $\{N,X\}$ and $\{N,Y\}$. These two sets of data are generalized to an equidistant domain: $\{N_{eq},X_{eq}\}$ and $\{N_{eq},Y_{eq}\}$ using interpolation. This concludes the first step of the four-step contour comparison method.
The second step involves a fast Fourier transformation. The vectors X_{eq} and Y_{eq} are transformed to vectors in the frequency domain:

$$\omega_X = FX_{eq} \qquad \omega_Y = FY_{eq} \tag{10}$$

The vectors are then multiplied with their conjugates, creating the vectors $n\omega_X$ and $n\omega_Y$ containing the frequency content. The first element in the frequency content vectors contains information about the average translation of the frequencies. This first element is discarded in both vectors thus making the remaining vectors independent of translation in the original domain.
The third step is about removing the influence of contour rotation. This is done by summation of the frequency content vectors creating the invariant:

$$n\omega_{XYi} = n\omega_{Xi} + n\omega_{Yi} \tag{11}$$

This computation eliminates the rotation dependency, because the summation of frequency remains constant when the contour is rotated in R^2 space.
The final fourth step is the interpretation of the results. For contour comparison the only interest lies in values that indicate resemblance between different sets of invariants. The commonly used smallest quadrant method, formula 12, is used in the experiments to determine the resemblance between sets of invariants.

$$E = \sum_{i=1}^{N} (n\omega_{XY1i} - n\omega_{XY2i})^2 \tag{12}$$

4.3 Introduction: Functionality 2

For the second functionality a number of optimization parameters are formulated. These can be used as plug-ins into the second functionality. The number and type of plug-ins necessary depend on the experiment requirements. For our sample experiment we have used the surface and the content plug-in.

4.4 Plug-in: Surface

The surface area of the calculation and measurements is based on summing the areas of their elements. Both the measurement and calculation results are given in a connected number of elements. The calculation plug in transforms the elements into triangular elements, calculates the area and successively sums these area's into the total area, as indicated the formula 13. The difference between measured and calculated area space is used as input for the optimization procedure.

$$Opp = \sum_{i=1}^{N} \frac{1}{2!} \begin{vmatrix} x1_i & y1_i & 1 \\ x2_i & y2_i & 1 \\ x3_i & y3_i & 1 \end{vmatrix} \tag{13}$$

4.5 Plug-in: Content

The content plug-in is an important optimization parameter, cause it enables the optimization of material values such as martensite. For the calculation of this parameter we used the element surface area from the surface plug-in, multiplied it by its mean material value. Summed the element content into total content, see formula 14. The difference between measurement and calculation total content is used as optimization parameter.

$$Content = \sum_{i=1}^{N} Opp_i * \overline{frac_i} \tag{14}$$

5 SAMPLE EXPERIMENT

The goal of the sample experiment is to converge the current state towards the prototype and optimize the material models ability to simulate martensite fraction throughout the cross section. The measured cross section of a metal forming process is used as prototype. A finite element model, using the Post Nanoflex material model, is used as current state.
For the first functionality the optimization procedure controls a number of process parameters: blank diameter, punch radius and indentation depth, blank radius and blank holder force. This optimization resulted in the convergence of the current state shape towards the prototype. Some snapshots of this convergence process are shown in figure 5. The resulting process parameters are then inserted into the second functionality.

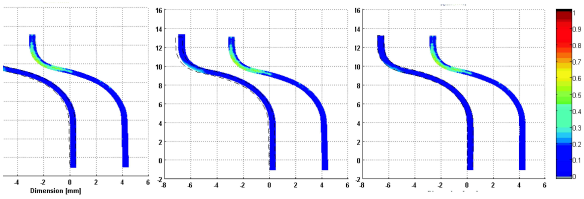

Figure 5: Convergence of shape. This figure shows three snapshots of the convergence of shape. The first snapshot on the left side is at the start of the convergence process, the middle snapshot is during the process and the snapshot on the right is the result of the process. The snapshots show two cross section: the left is the calculation and the right the measurement. The dashed outline is the contour of the measurement projected on the calculation to allow visual shape comparison.

For the second functionality a number of material model parameters are used to control the optimization: the influence of the hydrostatic stress on C_{strain}, the initial values of C_{strain} and C_{stress}. As optimization parameter the content difference of martensite between current and prototype state is used. This optimization resulted in the snapshots shown in figure 6.

6 CONCLUSIONS

- The experiment shows that the optimization method works and that it can be used to optimize material models.
- The experiment shows that an optimized Post Sandvik Nanoflex model is able to simulate the martensite content adequately within the optimization limits.
- For further improvement of the material model the optimization domain must be expanded to incorporate effects such as martensite bands.
- To optimize constitutive behavior of the model requires measurements on different stages and time steps after cold forming. Due to the transformation behavior.

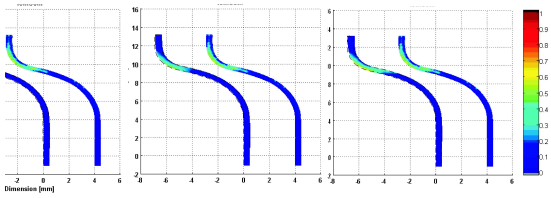

Figure 6: Convergence of martensite. This figure shows three snapshots of the convergence of shape. The first snapshot on the left side is at the start of the convergence process, the middle snapshot is during the process and the snapshot on the right is the result of the process. The snapshots show two cross section: the left is the calculation and the right the measurement. The dashed outline is the contour of the measurement projected on the calculation to allow visual shape comparison. The color bar ranges from zero to one martensite fraction

REFERENCES

[1] Post J. *On the Constitutive Behaviour of Sandvik Nanoflex, Modelling, Experiments and Multi-stage Forming.* ISBN 90-6464-974-X, University of Twente, 2004.

[2] M. Holmquist, J.-O. Nilsson, and A. Hultin Stigenberg. Isothermal formation of martensite in a 12Cr-9Ni-4Mo maraging stainless steel. *Scripta Metallurgica et Materialia*, pages 1367–1373, January 1995.

[3] J.-O. Nilsson, A.H. Stigenberg, and P. Liu. Isothermal formation of quasicrystalline precipitates and their effect on strength in a 12Cr-9Ni-4Mo maraging stainless steel. *Metallurgical Transactions A*, 25A:2225–2233, October 1994.

[4] V. Raghavan. Kinetics of martensite transformtions in the book martensite: A tribute to Morris Cohen, edited by G.B. Olson and W.S. Owen. *book*, (ISBN 0-87170-434-X):197–225, 1992.